

## CHAPTER 2

### LITERATURE REVIEW

This chapter mentions the basic knowledge concerning the dielectric, ferroelectric and thermal expansion significant details of a lead-free perovskite electroceramics used for prototype system in this study. It is necessary to describe the general background of  $(\text{Bi}_{0.5}\text{Na}_{0.5})\text{TiO}_3$  and  $(\text{Bi}_{0.5}\text{Na}_{0.5})\text{ZrO}_3$ , and the effects of Zr/Ti ratio at B-site on the properties of perovskite materials. Besides, important-basic knowledge concerning the dielectric, ferroelectric and thermal expansion properties of perovskite material is also mentioned in detail.

#### 2.1 Dielectric properties

##### 2.1.1 Dielectric constant

Most perovskite materials often show the dielectric properties. Dielectric material is an electrical insulator that can be polarized by an applied electric field. The important parameters for most applications of perovskite materials are the dielectric constant (or relative permittivity;  $\epsilon_r$ ) and dielectric loss (loss tangent or dissipation factor;  $\tan\delta$ ). The overall charge neutrality of material in an external field is described by:

$$D = \epsilon_0 E + P \quad (2.1)$$

The vacuum contribution caused by the externally applied electric field is represented by the term  $\epsilon_0 E$ , and the electrical polarization of the matter in the system is described by  $P$ .

For a pure dielectric response of the material, the polarization is proportional to the electric field in a linear approximation by

$$P = \varepsilon_0 \chi_e E \quad (2.2)$$

where the  $\chi_e$  is the electric susceptibility.

It follows from Equation (2.1) and (2.2) that

$$D = \varepsilon_0 E + \chi_e \varepsilon_0 E = (1 + \chi_e) \varepsilon_0 E \quad (2.3)$$

If the space between the plates is filled with a dielectric of susceptibility  $\chi_e$ , the capacitance is increased by a factor  $1 + \chi_e$ .

The permittivity  $\varepsilon$  of the dielectric is defined by

$$\varepsilon = \varepsilon_0 (1 + \chi_e) \quad (2.4)$$

where

$$\frac{\varepsilon}{\varepsilon_0} = 1 + \chi_e = \varepsilon_r \quad (2.5)$$

and  $\varepsilon_r$  is the relative permittivity (referred to as the dielectric constant) of the dielectric.

### 2.1.2 Dielectric loss

Dielectric loss can be defined in a current-voltage relationship for the charging and discharging capacitor, which is described with the help of a 'phasor' diagram (Fig. 2.1). When a perfect capacitor is under an alternating electrical field as shown in Fig. 2.1(a), the instantaneous current (a vertical line) leads the voltage (horizontal line) by  $90^\circ$ . In case of a real capacitor (Fig. 2.1(b)), it can be seen that the difference between current and voltage is less than  $90^\circ$ . The fraction of the product of the capacitive current (the component  $90^\circ$  out of phase with the voltage) and voltage is  $\tan \delta$  (dissipation factor). This term is due primarily to two factors, current leakage and dipole friction. Losses due to current leakage are low if the electrical resistivity is high. Dipole friction occurs when reorientation of the dipoles is difficult, as in complex organic molecules.

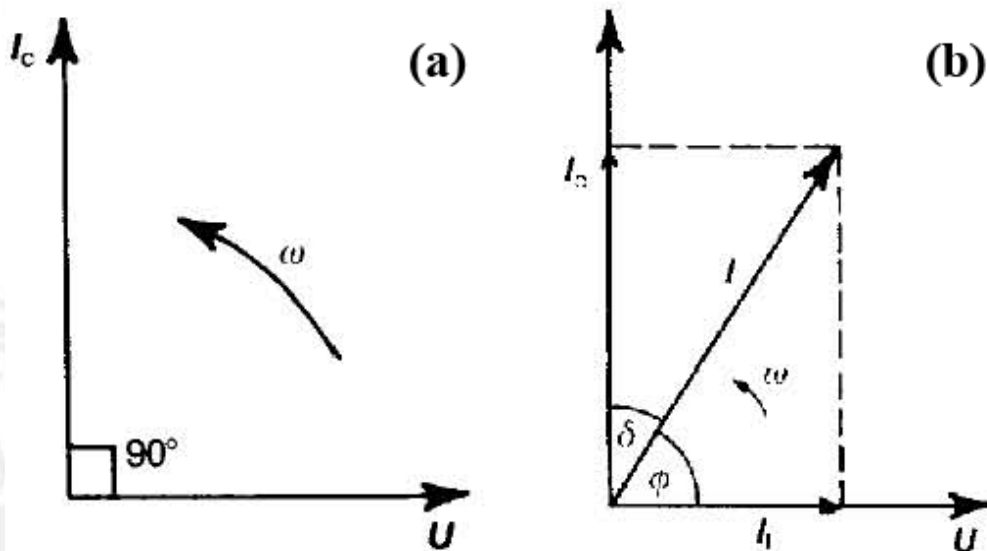


**Figure 2.1** Phasor diagram for (a) a perfect capacitor and (b) a real capacitor [10].

### 2.1.3 Frequency dependence of dielectric polarization

Polarization occurs due to four main atomic mechanisms i.e. a space charge contribution, which involves the diffusion of ions over several interact atomic distance, an orientational or dipolar contribution, which is built up of molecules possessing a permanent dipole moment, an ionic contribution in which comes from the displacement of ions over a small distance due to the applied field and electronic contribution, that comes from electrons in atom deforming the electron shell by the external electric field application. Figure 2.2 displays all the polarization process. The dielectric properties could be attributed to those mechanisms. When the dielectric material is under field with different frequencies, low-frequency dielectric behavior suggests the presence of all types of polarization mechanisms and that dipoles can follow the field so as to have high constant and low loss. Meanwhile, the higher frequency response shows that dipoles can no longer follow the field and consequently low dielectric constant and high dielectric loss result.

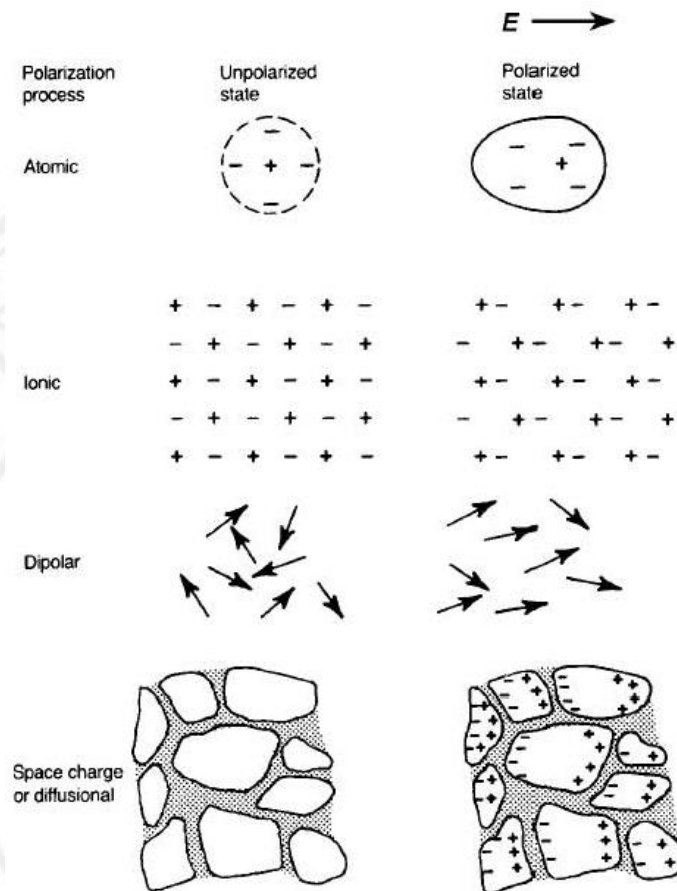


**Figure 2.2** Several polarization processes [10].

#### 2.1.4 Diffuse phase transition

From a temperature dependence of the dielectric study in normal ferroelectric materials, a phase transition point well known as the Curie point ( $T_c$ ) is generally sharp. However, it is possible that a transition temperature is not sharply defined. In this so-called diffuse phase transition temperature (DPT), the transition is usually induced by a chemical fluctuation and inhomogeneous sample. Besides, the broad phase transition is also a characteristic of relaxor ferroelectric materials governed by polar nano region mechanism (PNRs). Nevertheless, the diffuse dielectric peak found in both materials could be classified by investigating the dielectric properties as a function of the temperature with several frequencies. In most ferroelectrics, the

temperature as a function of the dielectric constant above the Curie point in which paraelectric phase dominales can be described by a simple raw called the Curie-Weiss law:

$$\varepsilon_r = \frac{C}{(T - T_o)} \quad (T > T_c), \quad (2.6)$$

where  $T_o$  is the Curie-Weiss temperature and  $C$  is the Curie-Weiss constant. The Curie-Weiss temperature is different from the Curie point. In case of  $T_o = T_c$ , the transition is second-order transition whereas the first-order phase transition occurs in case of  $T_o < T_c$ .

In relaxor materials and/or the materials showing the diffuse characteristics of ferroelectric-paraelectric phase transition, the maximum relative permittivity ( $\varepsilon_r$ ) does not obey the Curie-Weiss law. Thus, the deviation from the typical Curie-Weiss behavior of the materials can be described by a modified Curie-Weiss relationship in Eqn. 2.7 [11, 12]:

$$\frac{1}{\varepsilon_r} - \frac{1}{\varepsilon_m} = \frac{(T - T_m)^\gamma}{C}, \quad (2.7)$$

Where  $T_m$  is the temperature at maximum dielectric constant,  $\gamma$  and  $C$  are assumed to be constant. The parameter  $\gamma$  indicates the character of the phase transition: for  $\gamma = 1$ , a normal ferroelectric in which Curie-Weiss law is obtained,  $\gamma = 2$  described a complete diffuse phase transition suggesting the relaxor behavior [11].

## 2.2 Ferroelectric properties

### 2.2.1 Ferroelectric phases and domains

Ferroelectricity was discovered in 1921 by Valasek in Rochelle salt [13]. The ferroelectric phase can be defined as a state that shows spontaneous polarization which can be reoriented by an external applied electric field. The direction of individual spontaneous polarization dependent on crystal structure is illustrated in Fig. 2.3. The electric dipole alignment in the materials can occur in both uniform orientation and non-uniform orientation relating to the reverse direction i.e. in twinning. The area in which the uniform polarization exists is called “ferroelectric domain” while “the domain wall” is the name for the interface between two adjacent domains. In general, the defect and mechanical stress can result in the formation of domain in order to minimize electrostatic energy of the system. Fig. 2.4 shows the presence of  $180^\circ$  and non- $180^\circ$  domains due to the strain minimization within the system.

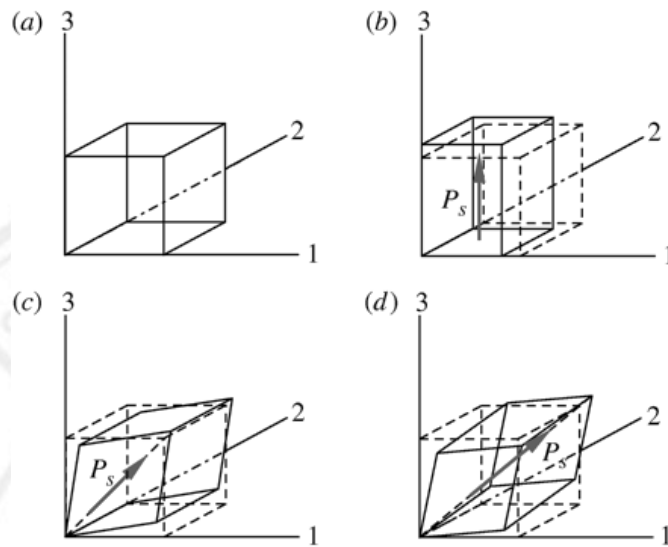


**Figure 2.3** Unit cells of the four phases (a) cubic, (b) tetragonal, (c) orthorhombic and (d) rhombohedral (the dotted lines in (b), (c) and (d) indicate the original cubic cell).

Arrows indicate the direction of the spontaneous polarization ( $P_s$ ) in each phase.

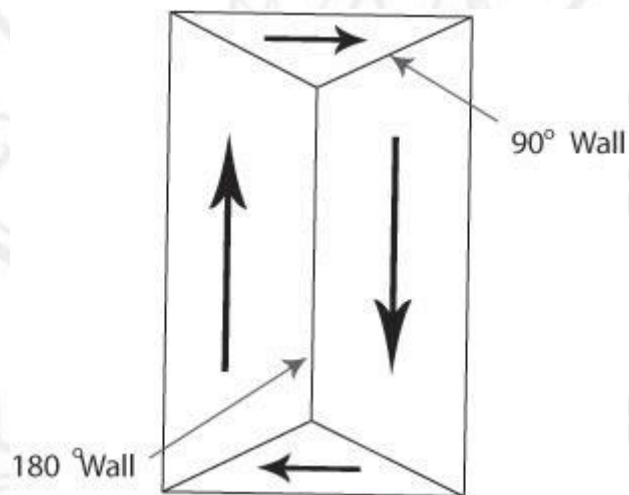


**Figure 2.4** Schematic illustrations of  $180^\circ$  and  $90^\circ$  domain walls [14].

### 2.2.2 Polarization switching and hysteresis loop

As an appropriate electric field is applied, the domain wall movement can produce single domain. The polarization within the domain can be reversed by high-enough applied field which is known as the polarization or domain switching. A measurement of the hysteresis polarization as a function of applied electric field as called  $P$ - $E$  hysteresis loop using simple circuit described by Sawyer-Tower [15] can reveal ferroelectricity in the materials. This behavior corresponds to the segment OA of  $P$ - $E$  loop in Fig. 2.5. As the electric field strength increases, the direction of the opposite domain will switch towards the field direction, which results in a rapid increment in polarization (segment AB). After that, all the domains are aligned and possibly reach a saturation state in segment BC. At this state, appropriately oriented crystals will be composed of a single domain. With the decrease of the field strength, the polarization will decrease as segment BD but does not go back to the origin. When the field is reduced to zero, the structure will display a remanent polarization ( $P_r$ ) involving the remains of aligned domains. The extrapolation of the linear segment BC of the hysteresis loop back to the polarization axis as CBE line indicates the spontaneous polarization ( $P_s$ ). At point F, the remanent polarization in a crystal cannot be completely removed until the applied field in the opposite direction reaches a certain value. The coercive field strength ( $E_c$ ) is required to reduce the polarization back to zero. Further, the increasing electric field in the negative (i.e. opposite) direction again causes the alignment of the dipole in this direction and the cycle is completed. Hence, the hysteresis loop (CDFGHC) is a representative of the relation between  $P$  and  $E$  shown in Fig. 2.5 [16, 17]. Nevertheless, many ferroelectric ceramics are not good insulators due to contribution of their conductivity in some

degree and high loss. The hysteresis loop characteristic of those ferroelectric ceramics is shown in Fig. 2.6 having an elliptical shape.

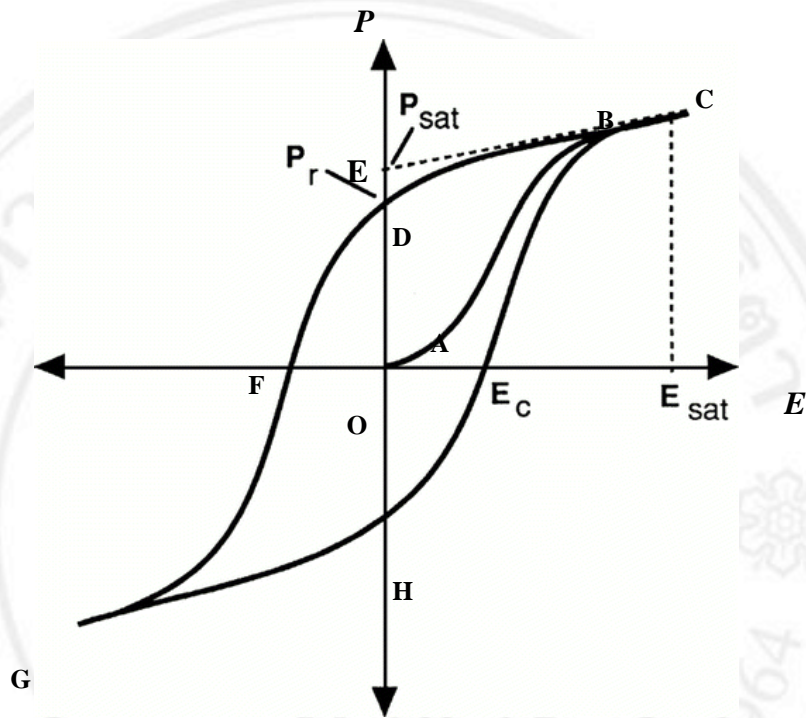


**Figure 2.5** A typical  $P$ - $E$  hysteresis loop in ferroelectrics [16, 17].

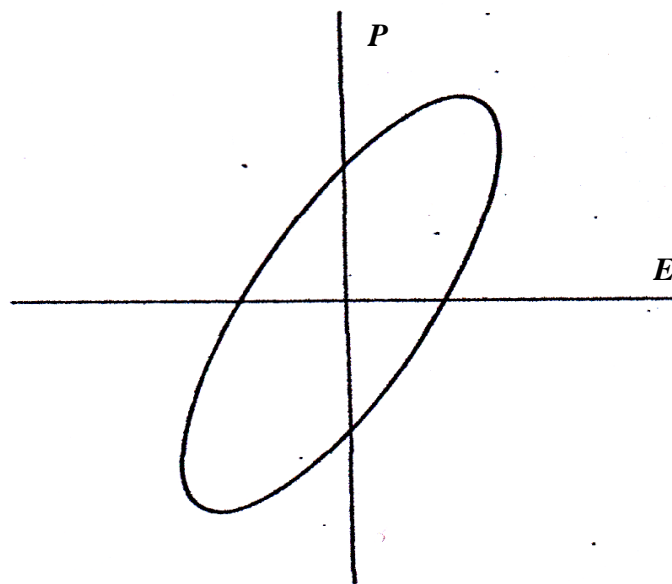


**Figure 2.6** Hysteresis loop for a lossy capacitor [7].

### 2.2.3 Hysteresis loop slope and area

From  $P$ - $E$  loops, the permittivity at high electric field (differential permittivity) attributed to reversible (intrinsic properties from lattice vibration and single-domain responses) and irreversible contribution (extrinsic domain-switching related property i.e. domain wall motion) can be calculated approximately [7] by using eqn. (2.8), which gives

$$\varepsilon = \frac{\Delta P}{\Delta E}, \quad (2.8)$$

where  $\varepsilon$  = the differential permittivity,

$\Delta E$  = applied field between +1 and -1 kV/cm,

$\Delta P$  = polarization difference between +1 and -1 kV/cm.

Dielectric properties at room temperature and low electric field mostly governed the reversible contribution while both reversible and irreversible governances provided the differential permittivity at high electric field. Besides, the  $P$ - $E$  loop area could indicate the polarization dissipation energy/hysteresis loss/energy loss of ferroelectric materials under one full cycle of electric field application. This amount of the energy loss is directly related to the amount of domains participating in the switching process during the application of electric field [18-20].

## 2.3 Thermal expansion

### 2.3.1 Thermal expansion coefficient

The coefficient of thermal expansion describes how the size of an object changes with a change in temperature. Specifically, it measures the fractional change in size per degree change in temperature at a constant pressure. Several types of coefficients have been developed: volumetric, area and linear. Which one is used depends on the particular application and which dimensions are considered important. For solids, one might be concerned with the change along the length. When an object is heated or cooled, its length changes by an amount proportional to the original length and the change in temperature. Linear thermal expansion coefficient of an object can be expressed as

$$\alpha = \frac{(L_{final} - L_{initial})}{L_{initial} (T_{final} - T_{initial})} \quad (2.9)$$

Where  $L_{initial}$  and  $L_{final}$  represents, respectively, the original and final lengths with the temperature change from  $T_{initial}$  to  $T_{final}$ .

### 2.3.2 Thermal strain

In case of solid materials with a significant length i.e. rods or cables, an estimate of the amount of thermal expansion can be described by the material strain, given by  $\varepsilon$  and defined as:

$$\varepsilon = \frac{L_{final} - L_{initial}}{L_{initial}} \quad (2.10)$$

Both thermal expansion coefficient and thermal strain are the characteristics of materials. Though being the same material, the differences in phase and crystal structure can induce different thermal expansion coefficient and thermal strain values. Thus, phase transition can be obtained using a plot of these thermal properties as a function of temperature.

## 2.4 Lead-free perovskite materials

The largest group of ferroelectric ceramics and related materials is based on oxide perovskite of general formula,  $ABO_3$ . In addition, Perovskite compounds can be synthesized with an extremely wide variety of combinations of chemical elements. Many perovskite electroceramic materials have been well documented for examples  $Pb(Zr,Ti)O_3$  and  $BaTiO_3$ . However, for lead-based materials, there is problem about pollution due to the fact that lead oxide vaporizes during processing and lead stays for a long time in the environment. Thus, lead-free perovskite materials therefore are of interest for development. In this section, it is appropriate to outline the significant background of  $Bi_{0.5}Na_{0.5}TiO_3$ ,  $Bi_{0.5}Na_{0.5}ZrO_3$  and  $Bi_{0.5}Na_{0.5}Zr_{1-x}Ti_xO_3$  ceramics.

### 2.4.1 Bismuth sodium titanate (BNT)

$Bi_{0.5}Na_{0.5}TiO_3$  compound was discovered by Smolenskii et al. in 1960 [21]. This system has a rhombohedral perovskite-like structure, with the  $Na^+$  and  $Bi^{3+}$  ions distributed randomly in the 12-fold coordination sites. BNT exhibited a diffuse phase transition from rhombohedral to tetragonal phase between  $200^\circ\text{C}$  and  $320^\circ\text{C}$  and from tetragonal to cubic phase at  $540^\circ\text{C}$  [22-25]. This system had problems in poling process due to its own large coercive field.

In 2009, the temperature dependences of dielectric constant and loss tangent of  $\text{Bi}_{0.5}\text{Na}_{0.5}\text{TiO}_3$  ceramics in temperature range of 25-500°C as shown in Fig. 2.7 were performed by Y. Hiruma et al. [26]. It could be seen that the result suggested the diffuse phase transition. In addition, the depolarization temperature and maximum dielectric constant were revealed at 187 and 325°C, respectively. However, when compared with prototypical relaxor ferroelectrics showing a diffuse phase transition phenomenon, BNT showed a few anomalous behaviors. For example, in the middle of the diffuse phase transition, the polarization relaxation is not observed while the structural change from rhombohedral to tetragonal occurs.

In 2011, J. Y. Yi et al. [27] reported  $P$ - $E$  loop of BNT ceramics as shown in Fig. 2.8. The study showed clearly that this material behaves as a normal ferroelectric at room temperature. Moreover, they also found the change in a singular point of the thermal expansion near 300°C from thermal expansion data in Fig. 2.9.

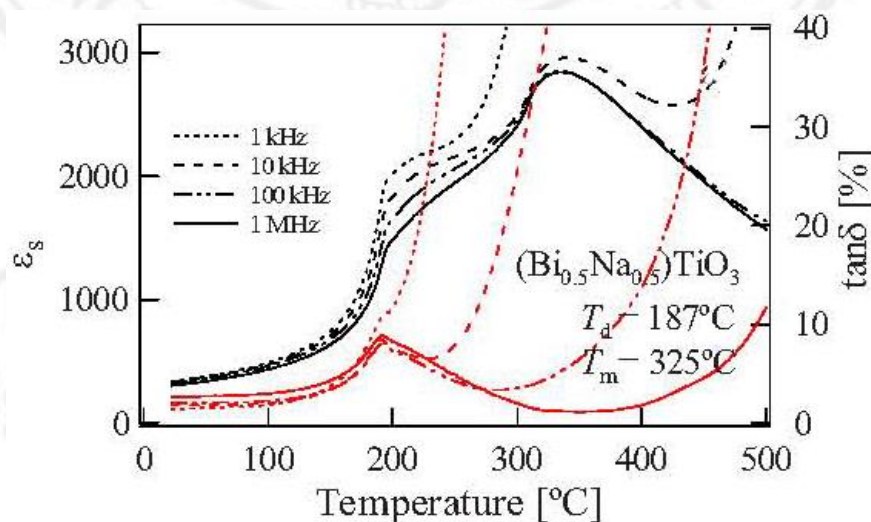


**Figure 2.7** Dielectric properties as a function of temperature of BNT ceramic [26].

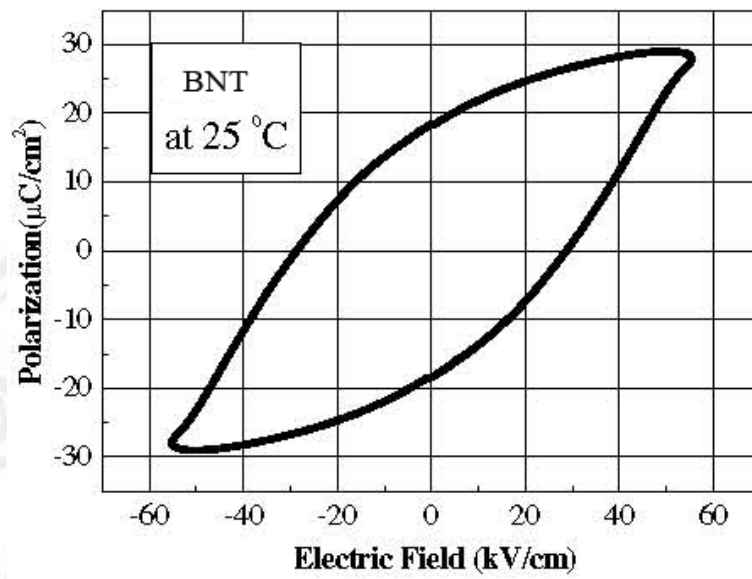


Figure 2.8  $P$ - $E$  loop of BNT ceramic [27].

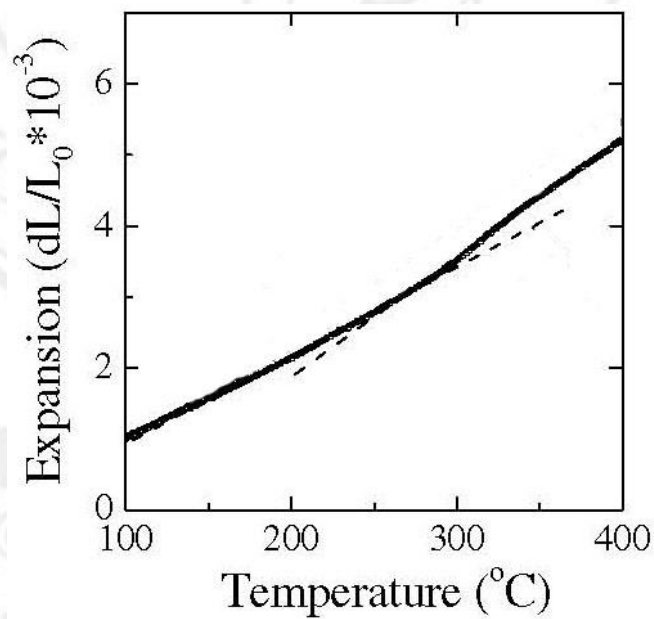
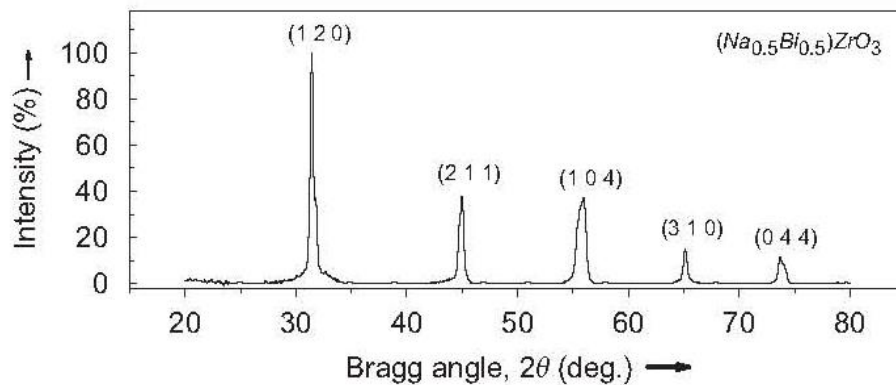


Figure 2.9 Thermal expansion of BNT ceramic [27].

### 2.4.2 Bismuth sodium zirconate (BNZ)

In 2007, K. Prasad et al. [28] fabricated successfully BNZ ceramic using a high-temperature solid state reaction method. The mixture and pellets were fired at 1070 and 1100°C for 4 and 3 h, respectively. As for structural study, a standard computer program (POWD), which was utilized for the XRD-profile analysis, revealed the single-phase orthorhombic structure. Figure 2.10 presents XRD pattern of this material at room temperature.



**Figure 2.10** X-ray diffraction pattern of BNZ ceramic [28].

In this report, a negative temperature coefficient of resistance (NTCR)-type behavior of this material was observed with the temperature dependence of real and imaginary parts of impedance at different frequencies as shown in Fig. 2.11. Besides, a decrease of the resistance for grain ( $R_g$ ) and grain boundary ( $R_{gb}$ ) in this material with increasing frequencies was found as pseudo Cole-Cole plots at 100 Hz, 1 and 10 KHz in Fig 2.12.

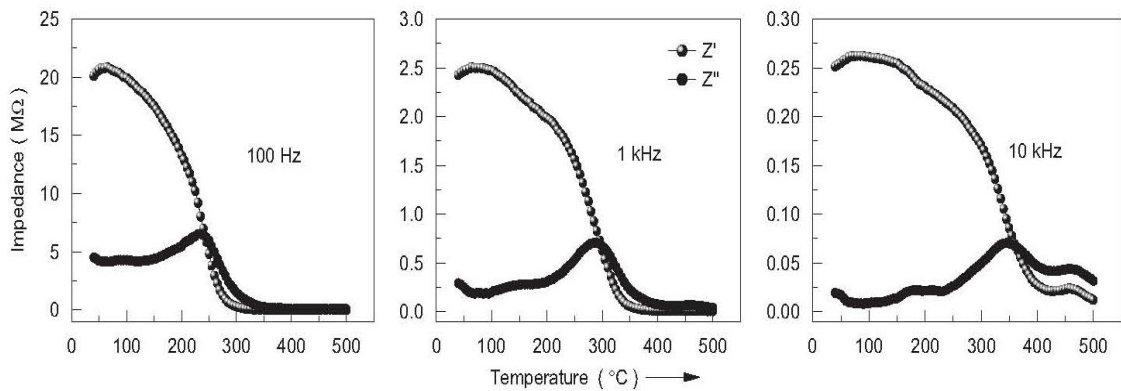


**Figure 2.11** Temperature dependence of real and imaginary parts of impedance of BNZ at different frequencies [28].

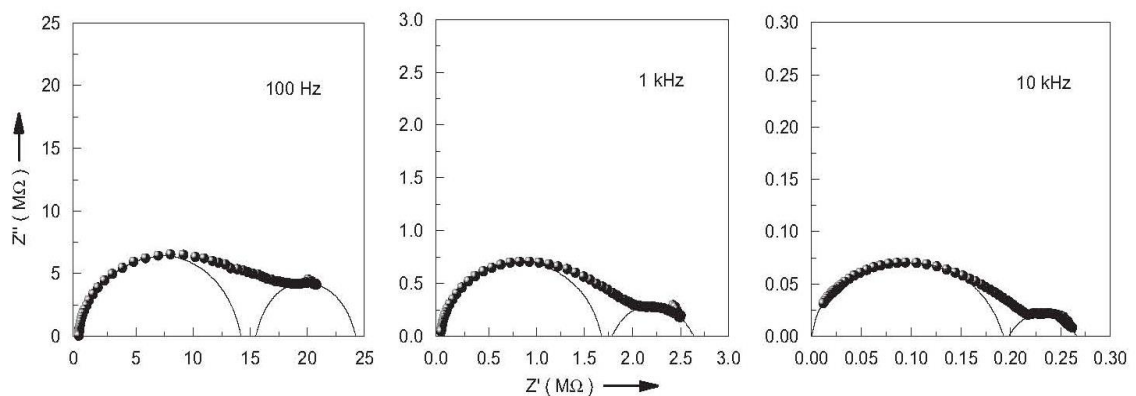


**Figure 2.12** Pseudo-Cole-Cole plot of BNZ at different frequencies [28].

### 2.4.3 Bismuth sodium zirconate titanate (BNZT)

During the past few years, several investigations suggested that modification at B-site plays an important role in tailoring various properties of perovskite materials [29]. Ion size difference was a significant factor to change microstructure and crystal structure leading to the enhanced properties of the ceramics. In this section, it is necessary to mention the important background science of modification at B-site using the different ions of  $\text{Ti}^{4+}$  and  $\text{Zr}^{4+}$  as  $\text{Bi}_{0.5}\text{Na}_{0.5}(\text{Zr},\text{Ti})\text{O}_3$  materials.

In 1995, Y. Yamada et al. mentioned the crystal structure and phase transition of BNZ-BNT system [30]. In the report, it suggested the rhombohedral structure for Ti-rich side. Besides, the phase transitional composition of this binary phase diagram for about  $\text{Bi}_{0.5}\text{Na}_{0.5}(\text{Zr}_{0.6}\text{Ti}_{0.4})\text{O}_3$  was also introduced. However, the phase appearing for Zr-rich side was not identified. The lattice parameter and phase transition temperature dependence of Zr content are shown in Fig. 2.13 and 2.14, respectively. It could be noticed that Zr addition resulted in the increase of lattice parameter and the decrease of phase transition temperature.

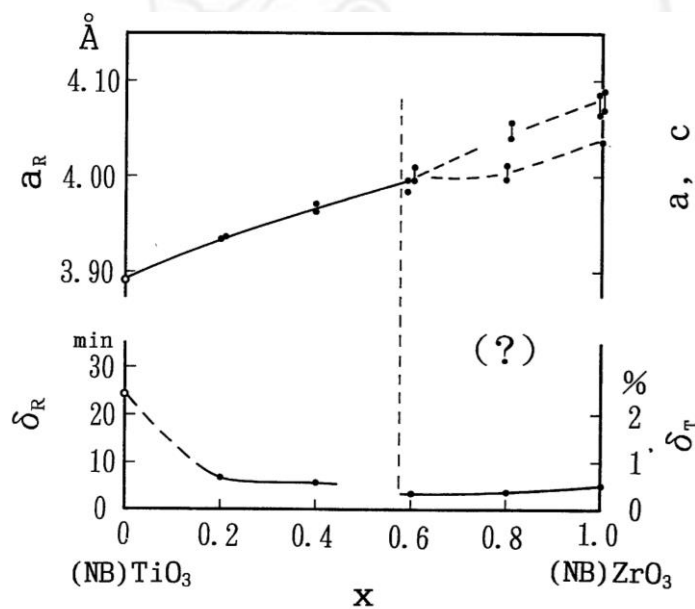


**Figure 2.13** Zr concentration dependence of lattice parameters of  $\text{Bi}_{0.5}\text{Na}_{0.5}\text{Ti}_{1-x}\text{Zr}_x\text{O}_3$  ceramics [30].

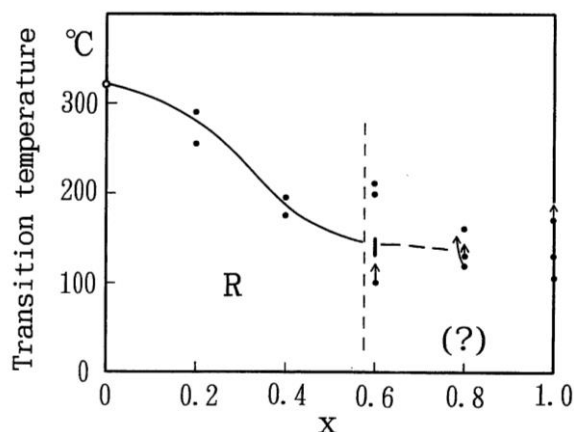


**Figure 2.14** Zr concentration dependence of transition temperature of  $\text{Bi}_{0.5}\text{Na}_{0.5}\text{Ti}_{1-x}\text{Zr}_x\text{O}_3$  ceramics [30].

The microstructures and mechanical properties of  $\text{Bi}_{0.5}\text{Na}_{0.5}(\text{Ti}_{1-x}\text{Zr}_x)\text{O}_3$  ceramics with Zr addition up to 0.2 mol% were reported by A. Watcharapasorn et al. in 2006 [31]. They guided that this addition did not change BNT rhombohedral structure. The slight grain size increment was observed with Zr increasing content. Regarding the mechanical properties, Knoop hardness and Young's modulus of BNZT ceramics as a function of Zr addition are shown in Fig. 2.15. It was seen that both values were increased with increasing Zr due to a variation of ionic size in the lattice moderately inhibiting the deformation caused by the hardness indenter and resulted in the increase in hardness and elastic modulus.

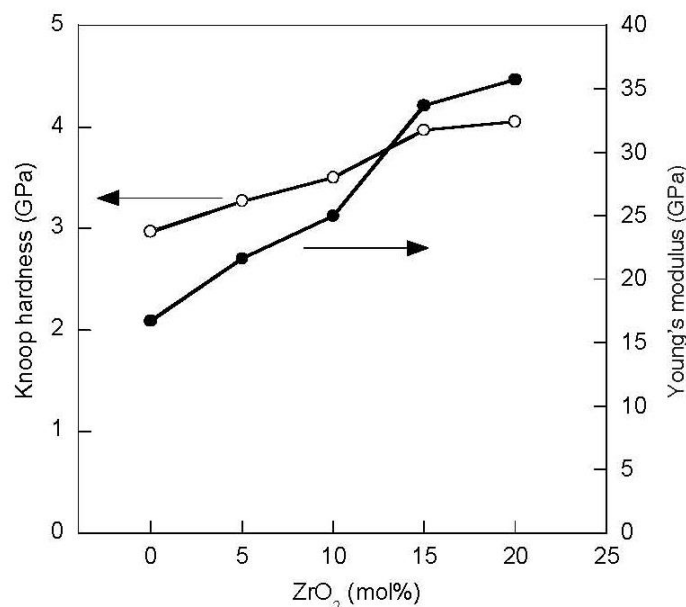


**Figure 2.15** Knoop hardness and Young's modulus of  $\text{Bi}_{0.5}\text{Na}_{0.5}\text{Ti}_{1-x}\text{Zr}_x\text{O}_3$  ceramics [31]

In 2008, A. Watcharapasorn et al. [32] reported further the dielectric properties of BNTZ ceramics as a function of temperature. The dielectric constant plotted as a function of temperature at 10 kHz is shown in Fig. 2.16. It could be seen that increasing Zr concentration caused the dielectric-temperature curves to become more diffused with corresponding lower values of high-temperature dielectric constant. The temperature dependence of dielectric loss of this system is shown in Fig. 2.17. The dielectric loss of all samples, except for 20 mol% of Zr content, showed a relatively constant value for all samples up to about 150°C. Above this temperature, the values slightly decreased and then increased as the loss became more significant at high temperature.

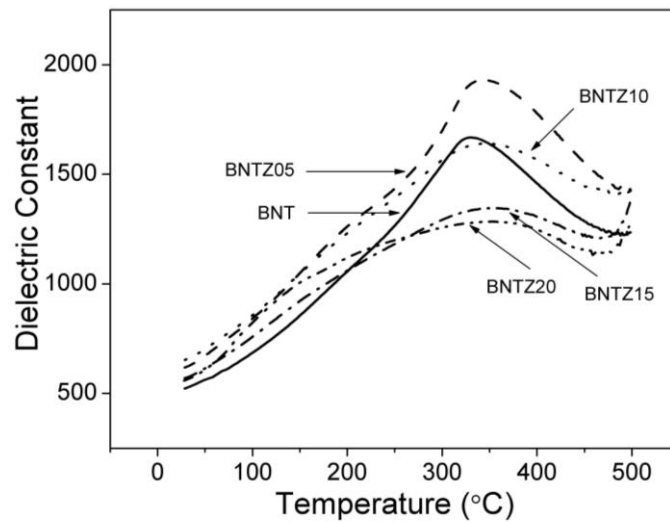


**Figure 2.16** Temperature dependence of dielectric constant at frequency of 10 kHz for  $\text{Bi}_{0.5}\text{Na}_{0.5}\text{Ti}_{1-x}\text{Zr}_x\text{O}_3$  ceramics [32].

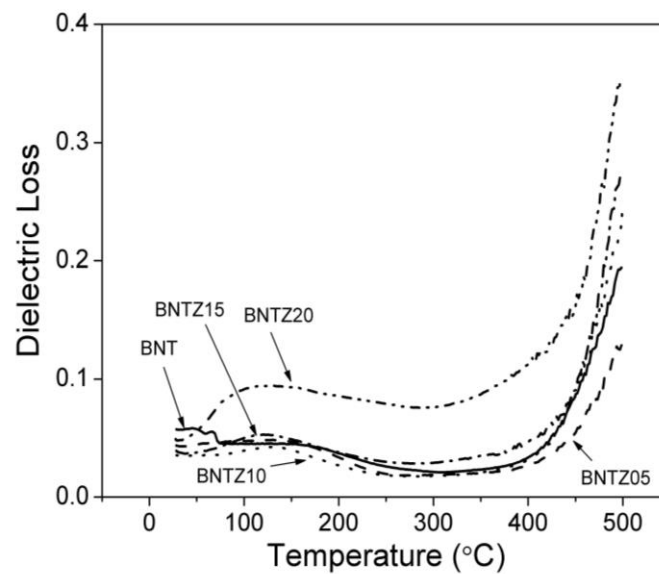


**Figure 2.17** Temperature dependence of dielectric loss at frequency of 10 kHz for  $\text{Bi}_{0.5}\text{Na}_{0.5}\text{Ti}_{1-x}\text{Zr}_x\text{O}_3$  ceramics [32].